

MRI Assessment of Hepatic Iron Clearance Rates After USPIO Administration in Healthy Adults

Pippa Storey, PhD,* Ruth P. Lim, MBBS, MMed, MS, FRANZCR,* Hersh Chandarana, MD,* Andrew B. Rosenkrantz, MD,* Daniel Kim, PhD,† David R. Stoffel,* and Vivian S. Lee, MD, PhD, MBA†

Objective: The purpose of this study was to monitor iron clearance from the liver by means of T2 and T2* mapping after administration of an ultrasmall superparamagnetic iron oxide (USPIO) agent.

Materials and Methods: The study was performed using ferumoxytol (Feraheme), a USPIO agent that has been approved by the US Food and Drug Administration for the treatment of iron deficiency anemia in adult patients with chronic kidney disease. Six healthy human participants without anemia or preexisting iron overload were prospectively included. The cohort comprised 4 men and 2 postmenopausal women, aged 22 to 57 years. T2 and T2* mapping of the liver were performed at 1.5 T using multiple spin echo and multiple gradient echo sequences, respectively. After baseline imaging, ferumoxytol was injected intravenously at a dose of 5 mg Fe/kg body weight. Imaging was repeated at 3 days, 1 month, and every 2 months thereafter for up to 11 months or until liver T2* had recovered to 24 milliseconds, the threshold used to define iron deposition. For each examination, maps of the relaxation rates R2 ($= 1/T2$) and R2* ($= 1/T2^*$) were generated by fitting the signal intensity data as a function of echo time to a monoexponential decay.

Results: No adverse reactions to ferumoxytol injection occurred. The magnetic resonance (MR) responses to ferumoxytol varied widely among the participants. Liver R2* increased from a mean value of 35.6 s^{-1} (range, $28.7\text{--}40.9 \text{ s}^{-1}$) at baseline to a mean value of 241 s^{-1} (range, $161\text{--}417 \text{ s}^{-1}$) 3 days after administration. Liver R2 increased from 19.4 s^{-1} (range, $16.6\text{--}23.8 \text{ s}^{-1}$) at baseline to 45.3 s^{-1} (range, $34.4\text{--}58.5 \text{ s}^{-1}$) at 3 days. There was also a large variation in iron clearance times. In 1 participant, MR relaxation rates had recovered to baseline by 3 months, whereas, in 3 participants, liver R2* remained elevated at 11 months ($R2^* > 55 \text{ s}^{-1}$, ie, $T2^* < 18 \text{ milliseconds}$). In these 3 participants, liver R2 also remained marginally higher at 11 months than corresponding baseline values.

Conclusions: Iron deposition in the liver after a 5 mg Fe/kg dose of ferumoxytol may alter signal contrast on MR images for several months after administration. This is an important consideration in the use of USPIO agents for diagnostic purposes.

Key Words: MRI, USPIO, ferumoxytol, iron, liver, spleen

(*Invest Radiol* 2012;47: 717–724)

Ultrasmall superparamagnetic iron oxide (USPIO) particles have attracted great interest as magnetic resonance imaging (MRI) contrast agents. Their small size, when combined with optimized coatings, produces high T1- and T2-relaxivities, allowing for either

positive or negative signal contrast.¹ Furthermore, their biodistribution and pharmacokinetics differ from those of gadolinium chelates, opening up a wide range of applications not possible with gadolinium.¹

Whereas conventional gadolinium-based contrast agents are eliminated by the kidneys through glomerular filtration, most USPIO particles are cleared from the blood by macrophages of the mononuclear phagocyte system. These macrophages exist primarily in the liver, the spleen, the bone marrow, and the lymph nodes. Because malignant cells do not take up the particles, a promising application of USPIO agents is magnetic resonance (MR) lymphography.² Meta-analyses of several lymphography studies have demonstrated that USPIO-enhanced MRI provides higher sensitivity and specificity for diagnosis of lymph node metastasis than either unenhanced MRI³ or gadolinium-enhanced MRI does.⁴

Because of their small size and long intravascular half-life, USPIO particles are also taken up by macrophages outside the mononuclear phagocyte system. These include macrophages associated with infection, inflammation, and immune-mediated disorders.⁵ Applications that exploit this property include characterization of atherosclerotic plaque⁶ and noninvasive detection of transplant rejection.⁷ USPIO uptake has been investigated both in animal models of atherosclerosis and in patient studies⁸ and was recently used as an outcome measure in a clinical trial to evaluate the effects of atorvastatin (Lipitor) on carotid plaque inflammation.⁹ Research has also focused on the use of USPIO-enhanced imaging as an alternative to biopsy for assessing renal¹⁰ and cardiac¹¹ allografts.

An important characteristic of any contrast agent is its elimination from the body. After the uptake of USPIO particles by macrophages, iron is released from the particle core within intracellular lysosomes and delivered into the body's iron pool, where it is stored in the form of ferritin and hemosiderin. Although iron is an essential nutrient, the body has limited means of excreting excess iron.^{12,13} This has potential implications for the application of USPIO-enhanced imaging as a monitoring tool because frequent administration of USPIO agents could result in iron accumulation. Another pertinent issue is the inadvertent effect of iron deposition on subsequent MR scans in terms of image quality and interpretation. Preclinical studies of iron elimination after USPIO administration have been performed in animal models,^{14–16} but, to our knowledge, no such data have previously been reported for humans.

The purpose of this study was to investigate clearance of iron from the liver in healthy adults after administration of a USPIO agent. The study was performed using ferumoxytol (Feraheme), which was approved for human use in the United States by the Food and Drug Administration in 2009. It is indicated for the treatment of iron-deficiency anemia in adult patients with chronic kidney disease but can be used off-label as an MRI contrast agent. In addition to having high T1- and T2-relaxivities, ferumoxytol can be administered by bolus injection. It has been tested in a variety of MRI applications, including vascular imaging¹⁷ and neuroimaging.¹⁸ In this study, iron uptake and clearance after ferumoxytol administration were monitored noninvasively by means of T2 and T2* mapping. These techniques have become standard clinical tools for evaluating tissue iron concentration

Received for publication May 1, 2012; and accepted for publication, after revision, July 30, 2012.

From the *New York University School of Medicine, New York, New York; and †University of Utah Health Sciences Center, Salt Lake City, Utah.

Conflicts of interest and sources of funding: This study was supported by grant HL092439 from the National Institutes of Health.

The authors report no conflicts of interest.

Reprints: Pippa Storey, PhD, Center for Biomedical Imaging, New York University School of Medicine, 660 First Ave, New York, NY 10016. E-mail: pippa.storey@nyumc.org.

Copyright © 2012 by Lippincott Williams & Wilkins

ISSN: 0020-9996/12/4712-0717

in patients with iron overload disorders.¹⁹ Imaging was performed in the liver because it is the primary repository of stored iron.^{13,20}

METHODS

Study Cohort

Participants were recruited prospectively under a protocol approved by the institutional review board of our medical center. Among the exclusion criteria were pregnancy, a history of anaphylactic reactions, and pre-existing iron overload as determined by baseline T2* imaging of the liver. A mean T2* shorter than 24 milliseconds at 1.5 T was used as the criterion for iron deposition.²¹ This is a very conservative threshold and excludes people with even mildly elevated iron levels. Of the 9 individuals who provided informed consent to participate, 3 were excluded. One had a history of multiple allergies, and 2 were found to have baseline liver T2* shorter than the threshold value. The remaining 6 individuals comprised 4 men and 2 postmenopausal women, aged 22 to 57 years. None reported having anemia or any chronic disease.

Contrast Agent

Ferumoxytol (AMAG Pharmaceuticals, Cambridge, Massachusetts) consists of a colloidal solution of iron oxide nanoparticles formulated with mannitol. Each nanoparticle comprises a superparamagnetic magnetite core of about 6.8 nm in diameter covered with a semisynthetic carbohydrate coating of polyglucose sorbitol carboxymethylether, giving the particle an overall size of 17 to 31 nm in solution. The coating isolates the bioactive iron from plasma components, allowing for safe bolus administration and resulting in an intravascular half-life of approximately 16 hours in humans.²² When used for its approved indication as an iron replacement therapy, the recommended dose of ferumoxytol is 2 intravenous injections of 510 mg of iron each, administered at an interval of 3 to 8 days. In the present study, a single dose of 5 mg Fe/kg body weight was used. Over our study cohort, this was equivalent to 318 to 501 mg of iron.

Study Protocol

Imaging was performed on a 1.5-T Avanto system (Siemens Medical Solutions, Erlangen, Germany), using a body phased array coil in combination with spine coil elements in the patient table for signal reception. The first scan was performed before USPIO administration and was used to screen for pre-existing iron overload and to collect baseline data. Ferumoxytol was injected as an intravenous bolus within 32 days of the initial scan, and imaging of USPIO uptake was performed 3 days later. This interval was chosen because it corresponded to approximately 5 times the reported plasma half-life of the agent and was therefore expected to coincide with peak macrophage uptake. To monitor subsequent iron elimination, further scans were conducted at 1 month and every 2 months thereafter for up to 11 months or until liver T2* had recovered to 24 milliseconds, the threshold used to define iron deposition. The participants were asked to complete a questionnaire at each visit concerning aspects of diet and lifestyle that may affect iron metabolism.

Image Acquisition

T2* mapping was performed during breath-hold using a single-slice 2-dimensional multiple gradient echo (MGRE) sequence with fat saturation. Thirty-two echoes were acquired in a single echo train with monopolar readout gradients, a minimum echo time (TE) of 1.3 milliseconds, and an echo spacing of 1.97 milliseconds. Each echo supplied data for a separate image, producing a total of 32 images with different TE values. Other acquisition parameters were as follows: receiver bandwidth (BW), 840 Hz/pixel; field of view (FOV), 400 mm; base resolution, 192; slice thickness, 9 mm; repetition

time (TR), 90 ms; and flip angle (FA), 15 degrees. An axial slice was prescribed at the level of the porta hepatis, and the resulting images were inspected for susceptibility artifacts from the lung or the bowel. The acquisition was typically repeated in 2 or 3 adjacent slices to ensure that at least 1 image set was relatively free of artifacts. At the 3-day and 1-month time points, when the signal decay was anticipated to be rapid, additional data were collected using a customized 2-dimensional gradient echo sequence with a minimum TE of 0.8 milliseconds and an effective echo spacing of 0.1 milliseconds. These values were achieved using asymmetric echoes and acquiring successive echoes after separate excitations. With this approach, a total of 56 echoes were acquired in interleaved fashion within a single breath-hold. We will refer to this approach as the "interleaved gradient echo" technique. Other parameters were as follows: receiver BW, 920 Hz/pixel; FOV, 400 mm; base resolution, 160; slice thickness, 9 mm; TR, 8.6 milliseconds; and FA, 10 degrees.

A relatively thick slice (9 mm) was chosen to achieve the very short echo times necessary to quantify rapid signal decay using the interleaved gradient echo technique. For consistency, the same thickness was also used for the MGRE sequence. To investigate the possible effect of slice thickness on T2* values, 4 participants underwent an additional scan, in which the MGRE sequence was run with 4 different slice thicknesses (6, 9, 12, and 15 mm). Six acquisitions over 3 axial planes were performed for each slice thickness, making a total of 24 image sets for each participant.

T2 mapping was performed during breath-hold using a single-slice 2-dimensional multiple spin echo sequence with dark-blood preparation and spectrally adiabatic inversion recovery (SPAIR) fat suppression. An axial slice was prescribed at the level that exhibited the fewest artifacts on T2* images. Sixteen echoes were acquired with minimum TE of 3.44 milliseconds and echo spacing of 3.44 milliseconds. The turbo factor was set to 1, which means that each echo was used to generate a separate image with different TE. Other acquisition parameters were as follows: BW, 919 Hz/pixel; FOV, 400 mm; base resolution, 160; slice thickness, 9 mm; and TR, 300 milliseconds with the restore pulse on. To ensure that data could be acquired within a single breath-hold, generalized autocalibrating partially parallel acquisition (GRAPPA) was applied with an acceleration factor of 2 and 24 reference lines.

Although the spleen was not the initial focus of the study, in many cases it lay within the FOV of the T2 and T2* acquisitions.

To estimate the volume of the liver, a 2-dimensional multislice T1-weighted gradient echo sequence with complete liver coverage was performed during breath-hold. Twenty-five contiguous axial slices with 10-mm thickness were acquired in interleaved order using the following imaging parameters: FOV, 400 mm; base resolution, 192; FA, 90 degrees; TR, 112 milliseconds; TE, 1.71 milliseconds; receiver BW, 470 Hz/pixel. The acquisition was performed at least twice in each participant to gauge measurement precision. The resulting images were also used to estimate the volume of the spleen.

Image Analysis

Maps of R2* ($= 1/T2^*$) were generated by fitting the gradient echo signal intensity as a function of TE to a monoexponential decay for each pixel in the FOV. All analyses were performed in Matlab (Mathworks, Natick, Massachusetts) using a nonlinear Levenberg-Marquardt algorithm. For pixels in which the intensity fell below twice the noise level before the end of the echo train, the remaining data points were automatically truncated. The noise level was estimated from an artifact-free region in the image background.

Maps of R2 ($= 1/T2$) were generated from the multiple spin echo images in an analogous manner. However, the noise level could not be measured from the image background because the use of parallel imaging rendered the noise statistics inhomogeneous over the FOV. Instead, an intensity threshold for data truncation was estimated

by inspection of a few representative decay curves, erring on the side of overestimation to avoid any possibility of bias in the R2 values.

Mean hepatic R2 and R2* values were obtained for each examination by averaging the respective 2-dimensional maps over the liver. Large vessels and localized susceptibility artifacts were masked out using a thresholding procedure. Slices that were severely corrupted by artifact were discarded. Because these steps involved a small amount of user input, the operator was blinded to the participant identity and time point, and aspects of the user interface such as intensity windowing were designed to minimize the likelihood of inadvertent identification. A similar analysis was performed for the spleen over all examinations in which the spleen was present in the FOV.

The volumes of the liver and the spleen were estimated by manually segmenting each slice of the T1-weighted gradient echo images. Segmentation was performed by a board-certified radiologist with 7 years of experience in abdominal imaging. The gallbladder was excluded from the liver volume, but intrahepatic vessels were included.

The 3-day responses to ferumoxytol, ΔR_2 and ΔR_{2^*} , were calculated by subtracting the baseline values of R2 and R2* from their respective 3-day values. In participants for whom both liver and splenic data were available, an integrated response over both organs was estimated using the following:

$$\int \Delta R \, dV \approx \Delta R_{\text{liver}} V_{\text{liver}} + \Delta R_{\text{spleen}} V_{\text{spleen}} \quad (1)$$

Here, ΔR denotes either ΔR_{2^*} or ΔR_2 and V is the volume of the organ. This equation assumes that the mean responses calculated from the 2-dimensional slices are representative of the entire organ.

Statistical Analysis

Correlations were calculated using Pearson's linear correlation coefficient. The sample size was too small to test whether the data were normally distributed. However, the t test of Pearson's correlation is known to be relatively robust to non-normality with respect to type I errors, and to have substantially greater statistical power at low sample size than its nonparametric equivalent, the exact test of Spearman's rank-order correlation.²³ Other statistical tests were applied as stated in the Results section. Significance was set at $P < 0.05$.

RESULTS

No adverse reactions to ferumoxytol injection occurred. The demographics and results of the volume measurements are summarized in Table 1. There was no significant correlation between the volumes of the liver and the spleen. Similarly, no significant correlations

were observed between the volume of either organ and the measures of body habitus, namely, weight, height, body mass index (BMI), or body surface area (BSA).

According to self-reported data, no participant donated whole blood within 4 months of the baseline examination or at any other time during the study period. However, participant 2 reported relatively frequent blood draws (on average, 1 per month) for other research studies. Participant 6 was a vegan, whereas the others consumed meat regularly. Participant 3 took oral iron supplements (16 mg/day) as part of a multivitamin regimen, whereas the others did not.

Image quality in the liver was satisfactory in all examinations. Slice thickness was found to have a small but significant effect on R2* according to 2-way analysis of variance ($P = 0.003$). Using the analysis method described earlier, in which regions exhibiting susceptibility artifact were segmented out, a mean R2* increase of 1.1 s^{-1} was observed for each 3-mm increase in slice thickness between 6 and 15 mm.

At the 3-day and 1-month time points, dephasing was sufficiently rapid in some participants that R2* was calculated from the interleaved gradient echo images instead of, or in addition to, the standard MGRE images. At day 3, the interleaved gradient echo images were used in 3 participants; the MGRE images, in 1 participant. In the remaining 2 participants, both acquisitions were used and the results were averaged. At the 1-month time point, the interleaved gradient echo acquisition alone was used in 1 participant, the MGRE images alone were used in 3 participants, and both acquisitions were used in 2 participants. For the 4 examinations in which both acquisitions were used, the interleaved gradient echo acquisition produced, on average, slightly higher R2* values than the MGRE acquisition did (mean difference, 2.2%; range, -0.6% to 4.5%). This trend, however, was not statistically significant according to either the Student t test ($P = 0.15$) or its nonparametric equivalent, the Wilcoxon signed rank test ($P = 0.25$). In the spleen, the interleaved gradient echo acquisition was used at the 3-day time point; the MGRE acquisition, at other time points.

Figure 1 shows R2* and R2 maps from participant 5 at each time point over the entire 11-month period of the study. Note that the color scales (shown on the left side of Fig. 1) differ between the R2* and R2 maps. R2* exhibits a dramatic increase in both the liver and the spleen at the 3-day time point ($\Delta R_{2^*} = 207 \text{ s}^{-1}$ in the liver and $\Delta R_{2^*} = 373 \text{ s}^{-1}$ in the spleen), whereas R2 shows a smaller rise ($\Delta R_2 = 24 \text{ s}^{-1}$ in the liver and $\Delta R_2 = 33 \text{ s}^{-1}$ in the spleen). Liver R2* and R2 both decline gradually over the following months, but neither has recovered fully to its baseline value by the final scan at 11 months. In the spleen, by contrast, 90% of the R2* recovery and 88% of the R2 recovery occur within the first month.

TABLE 1. Demographic Information and Results of Volume Measurements

Participant	Age/Sex	Weight, kg/Height, cm	BMI*	BSA, m^2 †	Liver Volume, mL‡	Splenic Volume, mL§
1	52/F	63.5/153	27.1	1.61	1610	84
2	41/M	80.3/160	31.4	1.84	1319	171
3	57/F	97.5/168	34.6	2.07	1501	148
4	25/M	100.2/176	32.5	2.16	1912	102
5	28/M	79.4/178	25.1	1.97	1668	161
6	22/M	71.7/179	22.5	1.89	1895	353

*Body mass index is equal to (weight [kg])/(height [m])².

†Body surface area, calculated according to the formula of Dubois & Dubois, ie, BSA [m^2] = 0.007184 × (weight [kg])^{0.425} × (height [cm])^{0.725}.

‡The precision of the liver volume measurement is estimated at $\pm 20 \text{ mL}$.

§The precision of the splenic volume measurement is estimated at $\pm 3 \text{ mL}$.

F indicates female; and M, male.

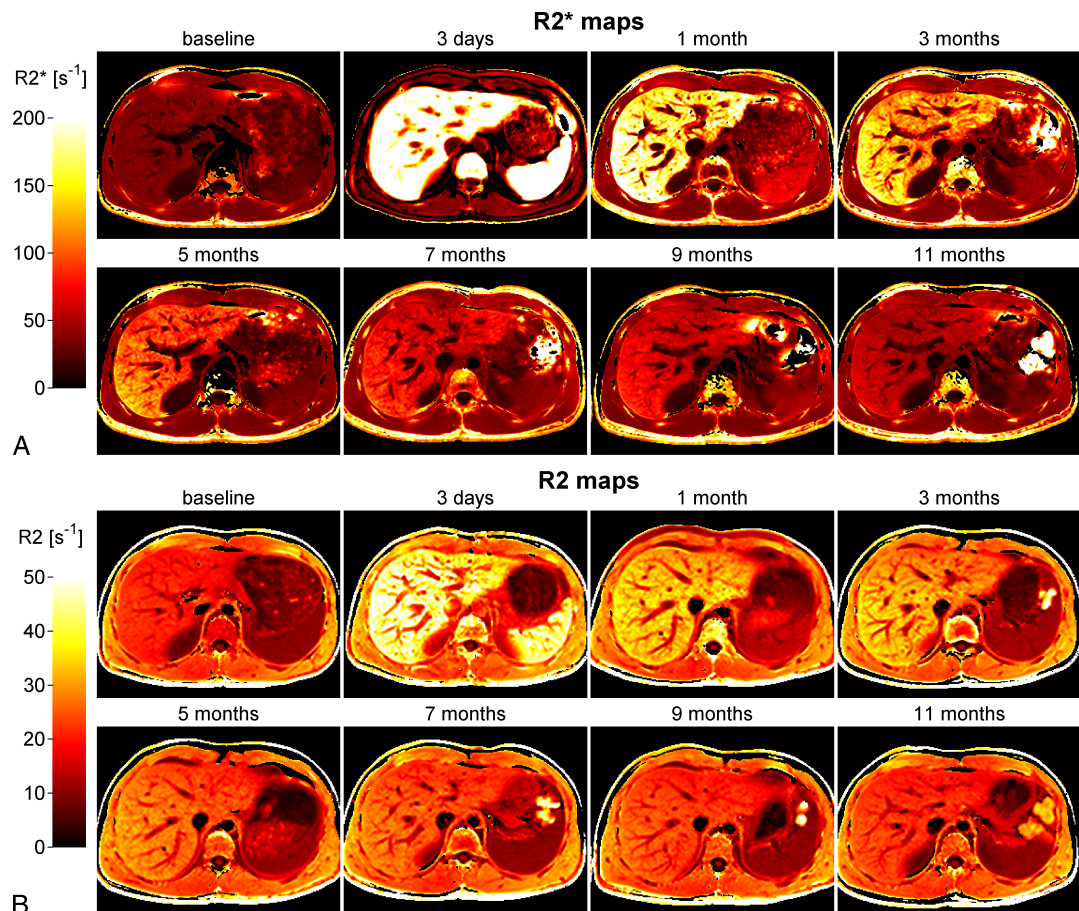


FIGURE 1. R2* maps (A) and R2 maps (B) from participant 5 at each time point over the entire 11-month period of the study. Note that the color scales (shown on the left side) differ between the R2* and R2 maps. Regions that have low signal on the first echo, such as background, have been made black. The R2* map shown for the 3-day time point was generated from the interleaved gradient echo images, with 0.1-millisecond effective echo spacing, whereas the remaining R2* maps were calculated from the conventional multiple gradient echo (MGRE) images, with 1.97-millisecond echo spacing. Note that R2* exhibits a dramatic increase in both the liver and the spleen at 3 days post-ferumoxytol. The R2 maps (B) also demonstrate a large response, although the increase in R2 is not as great as that in R2*. Liver R2* and R2 decline very slowly over the remainder of the study period, and neither has recovered completely to its baseline value at 11 months. By contrast, R2* and R2 in the spleen recover much more rapidly.

The upper graphs of Figure 2 show mean R2* and R2 values in the liver for all study participants as a function of time after ferumoxytol administration, with baseline values plotted at time zero. Note that the ranges on the vertical axes differ between the R2* and R2 graphs. The horizontal line on the R2* graph indicates the threshold used to define iron deposition ($T2^* = 24$ milliseconds, ie, $R2^* = 41.7 \text{ s}^{-1}$). R2* has a mean baseline value over the study cohort of 35.6 s^{-1} (range, $28.7\text{--}40.9 \text{ s}^{-1}$) and increases to 241 s^{-1} (range, $161\text{--}417 \text{ s}^{-1}$) at 3 days after the ferumoxytol injection. The 3-day response varies widely among the study participants, from $\Delta R2^* = 132 \text{ s}^{-1}$ in participant 6 to $\Delta R2^* = 381 \text{ s}^{-1}$ in participant 3. Although these 2 participants had the lowest and highest BMI, respectively, the correlation between BMI and $\Delta R2^*$ did not reach statistical significance ($r = 0.69$; $P = 0.13$). Neither was there a significant correlation between body weight and $\Delta R2^*$ ($r = 0.68$; $P = 0.14$).

In all participants, liver R2* exhibited a relatively sharp decline between 3 days and 1 month, followed by a gradual recovery that was well approximated by a monoexponential function. These features are illustrated in Figure 3, which displays R2* elevation for participant 3 on a logarithmic scale. The half-life associated with the

recovery varied widely among the participants, with a mean of 92 days and a range of 16 to 188 days. The time for complete elimination of excess iron reflected this variation (see Fig. 2A). In 1 person (participant 1), R2* had recovered to the threshold value by 3 months, whereas, in 3 individuals (participants 3, 4, and 5), R2* remained elevated at 11 months ($R2^* > 55 \text{ s}^{-1}$ ie, $T2^* < 18$ milliseconds). Participants 2 and 6 had recovered to the threshold value by 5 and 9 months, respectively.

The R2 results in the liver among all participants are shown in Figure 2B. Taking into account the smaller range of the vertical axis in Figure 2B compared with that in Figure 2A, it is clear that R2 is much lower than R2* at all time points. R2 had a mean baseline value over the study cohort of 19.4 s^{-1} (range, $16.6\text{--}23.8 \text{ s}^{-1}$) and increased to 45.3 s^{-1} (range, $34.4\text{--}58.5 \text{ s}^{-1}$) at 3 days. The 3-day response ranged from $\Delta R2 = 17.8 \text{ s}^{-1}$ in participant 6 to $\Delta R2 = 39.9 \text{ s}^{-1}$ in participant 3 and was significantly correlated with $\Delta R2^*$ ($r = 0.95$; $P = 0.004$). The recovery times of R2 also mirrored those of R2*; in participant 1, R2 had returned to baseline at 3 months, whereas, in participants 3, 4, and 5, R2 remained marginally higher at 11 months than corresponding baseline values. Among these 3 participants, the

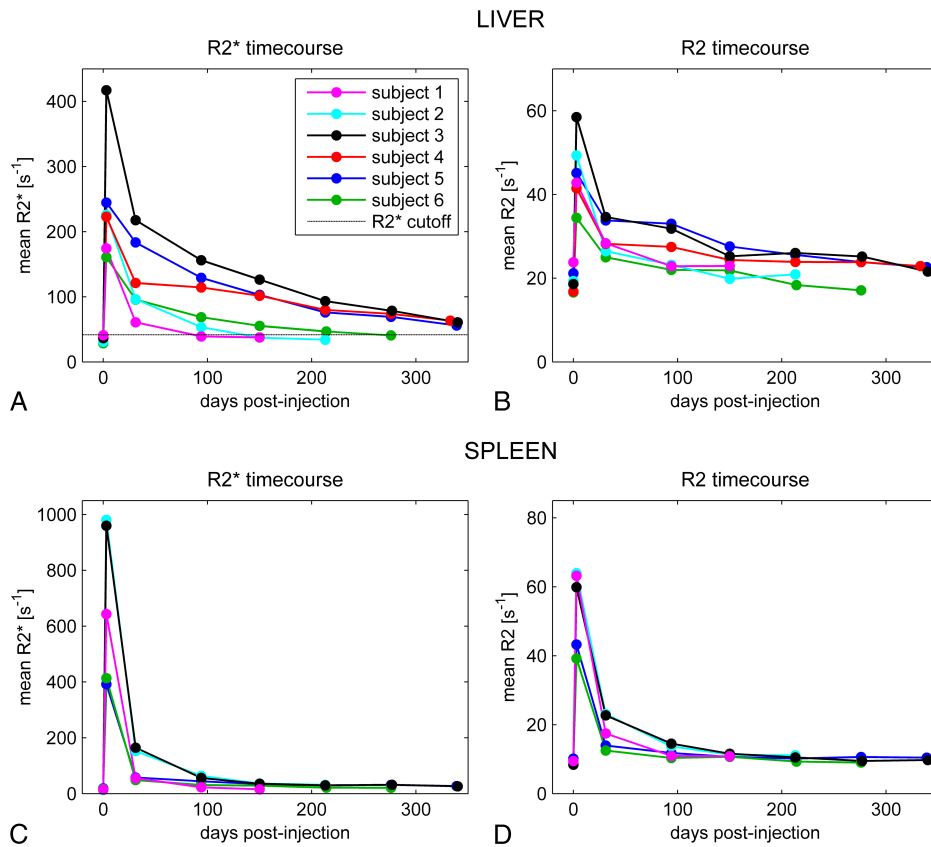


FIGURE 2. A to D, Graphs of R2* and R2 in the liver and in the spleen as a function of time after ferumoxytol administration, with baseline values plotted at day zero. Note that the ranges shown on the vertical axes differ among the graphs, being higher for R2* than they are for R2 and higher in the spleen than in the liver. The horizontal line in (A) marks the threshold used to define iron deposition in the liver ($T_2^* = 24$ milliseconds, ie, $R_2^* = 41.7 \text{ s}^{-1}$). Note that R2* and R2 increase sharply at 3 days both in the liver and in the spleen, although the response differs widely among the participants. R2* and R2 both recover slowly in the liver, with 3 participants still exhibiting elevated values 11 months after administration. In the spleen, the 3-day responses are greater than those in the liver, but the recovery is much faster.

residual R2 elevation above baseline averaged 3.5 s^{-1} , which was not substantially larger than the standard deviation over the entire cohort at baseline ($SD = 2.7 \text{ s}^{-1}$).

Figure 4 shows the relationship between R2 and R2* in the liver among all participants and all time points. With the exception of the 3-day data, R2 seems to exhibit a curvilinear dependence on R2*, increasing more slowly with R2* at higher R2* values. The 3-day results all lie above the line of best fit for the remaining data, suggesting that the relationship between R2 and R2* differs in the days immediately after ferumoxytol administration.

In the spleen, the R2* and R2 time courses could be estimated in all individuals except participant 4, whose images at several key time points did not include the spleen. The results are shown in Figures 2C and 2D. Among the 5 participants who were analyzed, R2* consistently exhibited a much larger 3-day response to ferumoxytol in the spleen (mean ΔR_2^* , 662 s^{-1} ; range, $373\text{--}968 \text{ s}^{-1}$) than it did in the liver (mean ΔR_2^* , 210 s^{-1} ; range, $132\text{--}381 \text{ s}^{-1}$). R2* also underwent greater recovery during the first month in the spleen (mean, 89%; range, 84%–94%) than it did in the liver (mean, 56%; range, 30%–83%). R2 showed a similar trend, exhibiting a larger 3-day response to ferumoxytol in the spleen (mean ΔR_2 , 44.7 s^{-1} ; range, $30.2\text{--}54.8 \text{ s}^{-1}$) than that it did the liver (mean ΔR_2 , 26.1 s^{-1} ; range, $17.8\text{--}39.9 \text{ s}^{-1}$) and undergoing greater recovery during the first month in the spleen (mean, 82%; range 72%–88%) than it did in the liver (mean, 62%; range, 47%–76%). The splenic response was

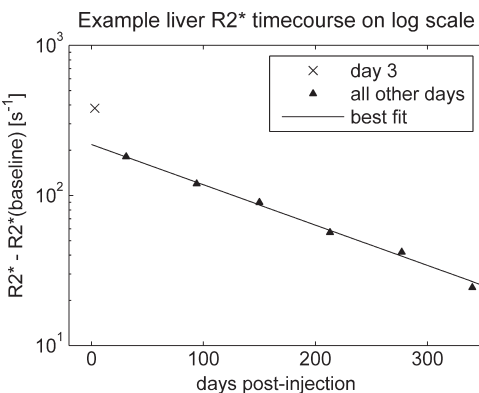


FIGURE 3. Example time course showing R2* elevation above baseline on a logarithmic scale. Data correspond to liver measurements in participant 3 and are identical to those shown in Figure 2A. Note the monoexponential character of the R2* recovery from the 1-month time point onwards and the deviation of the 3-day value (cross) from the line of best fit for the later data (triangles). For this participant, R2* was calculated from the interleaved gradient echo acquisition at both the 3-day and 1-month time points and from the MGRE images at all other time points.

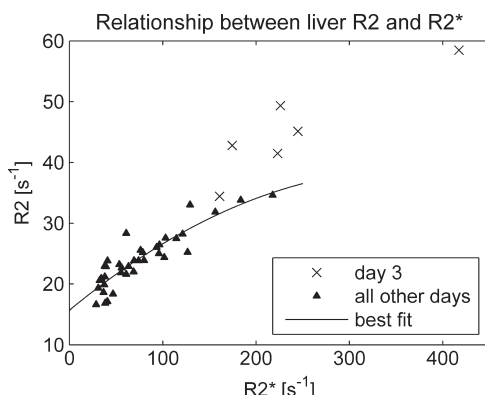


FIGURE 4. Graph of R2 versus R2* in the liver for all participants at all time points. Data from day 3 are plotted with crosses, whereas data from all other time points (baseline and 1 month onwards) are displayed using triangles. With the exception of the 3-day results, the data seem to exhibit a curvilinear relationship between R2 and R2* and have been fit using a second-order polynomial. The 3-day data all fall above the resulting line of best fit, suggesting that the relationship between R2 and R2* differs in the days immediately after ferumoxytol administration.

not significantly correlated with the liver response, as measured by either $\Delta R2^*$ or $\Delta R2$ ($P = 0.3$ and 0.4 , respectively). However, the integrated response over the liver and the spleen, defined in equation 1, was significantly correlated with the net dose of ferumoxytol in units of milligrams of iron. This was true for both the integrated $R2^*$ response ($r = 0.97$; $P = 0.006$) and the integrated R2 response ($r = 0.98$; $P = 0.004$).

DISCUSSION

Clearance of iron is an important consideration in the use of USPIO agents for diagnostic purposes. Although iron is an essential nutrient, required for the production of hemoglobin, myoglobin, and cytochromes, most of the body's needs are met through recycling of senescent erythrocytes by the mononuclear phagocyte system.¹² Of the 4 g of iron contained in the body of a typical adult man, only about 1 mg is lost per day, mainly through sloughing of cells from the skin and the mucosal lining of the gastrointestinal tract; in women with regular menstrual periods, the loss is slightly higher, averaging about 1.5 to 2 mg per day. These losses are offset by absorption of dietary iron, which is regulated by hepcidin through a feedback mechanism.^{12,13} Although the body can control intestinal absorption of iron, it has limited means of excreting excess iron.^{12,13} The lack of efficient excretion mechanisms underlies the pathological iron accumulation that occurs in patients with iron absorption disorders, such as hemochromatosis, or transfusion-dependent hemoglobinopathies, such as thalassemia.

The present study was conducted in healthy adults without anemia or pre-existing iron overload, using a single injection of ferumoxytol at a dose of 5 mg Fe/kg body weight. For comparison, the dose of ferumoxtran-10 (Combidex/Sinerem) that has typically been used for imaging lymph nodes and atherosclerotic plaque is 2.6 mg Fe/kg per scan. However, imaging applications of USPIO agents often require multiple scans to monitor disease progression or to test the effectiveness of a therapy. For example, the pre- and post-treatment

paradigm used by Tang et al⁹ to investigate the effectiveness of statin therapy involved 3 scans at intervals of 6 weeks, with a dose of 2.6 mg Fe/kg ferumoxtran-10 each time. This gave a net dose of 7.8 mg Fe/kg, which is 56% higher than that used in the present study.

Iron uptake and clearance were monitored noninvasively in this study using R2 and R2* mapping. These techniques have become accepted clinical tools for evaluating tissue iron concentration in patients with iron overload disorders. Although the quantitative effect of intracellular iron on R2 and R2* values depends on its molecular form and degree of aggregation,^{24,25} data from patients with transfusion-dependent thalassemia and sickle-cell disease have demonstrated a linear relationship between R2* and hepatic iron concentration up to 32.9 mg/g dry weight.²⁶ R2, by contrast, is known to exhibit a nonlinear dependence on hepatic iron concentration; it is less sensitive to iron deposition than R2* is, and its sensitivity decreases progressively as iron concentration increases.²⁶ A biophysical explanation for these findings has been suggested in terms of the distribution and clustering of ferritin and hemosiderin within cells of the liver.²⁷ It is reasonable to suppose that similar relationships between R2*, R2, and iron concentration will exist in the liver after the breakdown of USPIO particles into ferritin and hemosiderin. Indeed, the characteristic nonlinear relationship between R2 and R2* can be discerned in our results after excluding the 3-day time point. The 3-day data seem to differ from the rest, both in their relationship between R2 and R2* (shown in Fig. 4) and in their deviation from the monoexponential time course described by later data points (illustrated in Fig. 3). These observations suggest differences in the distribution and molecular form of the iron between day 3 and later time points. A possible interpretation is that the magnetite core of the USPIO particles remains largely intact at 3 days but is fully degraded into ferritin and hemosiderin by 1 month. The fact that USPIO particles have much higher magnetization than do their degradation products²⁵ could explain the elevation of R2* at 3 days above the otherwise monoexponential recovery time course (illustrated in Fig. 3).

Two notable results from our study were the wide variation in iron clearance rates among individuals and the extremely long time (>11 months) taken for complete elimination of excess iron in 50% of our study cohort (participants 3–5). In each of these individuals, R2* values remained above 55 s⁻¹ (ie, T2* < 18 milliseconds) at 11 months. In the other participants, recovery to the threshold value of R2* = 41.7 s⁻¹ (ie, T2* = 24 milliseconds) occurred earlier: in participant 6, by 9 months; in participant 2, by 5 months; and in participant 1, by 3 months. The slightly shorter clearance time observed in participant 6 may be because he was a vegan; he also had the lowest baseline R2* (28.7 s⁻¹). The much faster clearance in participants 1 and 2, however, cannot be fully explained by the dietary and lifestyle information gathered from the questionnaire. Participant 2 underwent frequent blood draws, but it is unlikely that the number reported (approximately 1 per month) can fully account for his faster iron clearance. In the case of participant 1, no explanation for the rapid elimination was apparent from the self-reported data. It is possible that the physiological basis for these differences in iron clearance rate may be related to genetic factors, which were beyond the scope of the study.

To our knowledge, this is the first investigation of iron clearance after USPIO administration in humans. Although studies have been performed in animal models,^{14–16} it is known that iron turnover differs markedly among species. In mice, for example, the amount of iron lost per day is similar to their total daily erythropoiesis needs, whereas, in humans, it accounts for only 5% to 10%, the remainder being recovered through iron recycling mechanisms.¹² Such differences in iron metabolism make it difficult to translate the results of animal studies to humans.

The long clearance times that we observed are an important consideration in the use of USPIO particles as contrast agents, both in terms of physiological iron burden and in regard to inadvertent effects

on subsequent MR examinations. The risk of iron toxicity from a single injection is extremely low, even for our heaviest participant, the 5 mg Fe/kg dose that we administered amounted to only 0.5 g, which is a small fraction of the iron load known to cause symptoms. However, chronically elevated levels of iron can lead to tissue injury through oxidative damage,^{13,28} and this may limit the frequency with which USPIO agents can safely be administered if used for purely diagnostic purposes. Furthermore, our results for R2 and R2* demonstrate that USPIO agents may affect signal contrast on subsequent MR examinations of the liver for several months after administration. Depending on the acquisition technique, iron deposition may degrade image quality or it may affect interpretation of the images, particularly if the radiologist is unaware that the patient has received intravenous iron. Diffusion-weighted images, for example, may be degraded because they have inherently low signal and are especially vulnerable to susceptibility artifacts. Iron deposition will further attenuate the signal and may introduce image artifacts because of the high magnetic susceptibility of the iron-storage proteins.

Iron deposition resulting from USPIO administration also presents a potential pitfall in image interpretation because it mimics iron overload disorders such as hemochromatosis. It has been shown that patients with a histopathologic iron grade of 3 or greater can be identified using a T2* cutoff of 14 milliseconds (ie, $R2^* = 71 \text{ s}^{-1}$).²¹ By interpolation of our data, we can deduce that it took a mean of 5.7 months (range, 1–10 months) from the time of ferumoxytol injection for liver R2* to recover to this cutoff value over our study cohort.

Another effect of iron deposition is to complicate estimation of liver fat. A routine approach used by radiologists to assess liver steatosis using MRI involves evaluation of the so-called fat fraction (FF).²⁹ This is calculated from the signals on in-phase and opposed-phase gradient echo images (S_{IP} and S_{OP} respectively) using the formula $FF = (S_{IP} - S_{OP}) / (2S_{IP})$. Iron deposition alters the relative amplitudes of the in-phase and opposed-phase images, thereby corrupting the estimate of fat fraction. A 10% change in relative amplitude, for example, will occur if $R2^*$ is increased by 44 s^{-1} above normal to a value of $R2^* = 80 \text{ s}^{-1}$. In our study, it took a mean of 4.6 months (range, 1–9 months) from the time of ferumoxytol injection for liver R2* to recover to this value.

USPIO administration will also affect signal contrast on T2-weighted fast spin echo images, which are commonly used to identify focal liver lesions and to detect hepatic inflammation or edema. Because iron will be stored only in macrophages and hepatocytes and not in tumor cells, it may actually increase the conspicuity of malignant nodules, and USPIO agents have, in fact, been advocated for this purpose.³⁰ On the other hand, the signal loss associated with iron deposition may mask T2 brightening associated with inflammation or edema. More generally, USPIO administration may pose challenges for diagnosis by altering the characteristic signal features used by radiologists to distinguish different types of pathology.

Although the spleen was not the focus of the study, we were able to analyze splenic data in all but 1 of our participants. The most notable finding was that the spleen exhibited consistently higher R2 and R2* responses than did the liver at the 3-day time point and greater recovery at 1 month. These results suggest that the spleen plays an important role in the uptake and catabolism of ferumoxytol particles but a lesser role in storing the iron released from the particle core. This interpretation is consistent with existing knowledge about the biodistribution and degradation of USPIO particles. Although the uptake distribution of iron oxide particles among different organs depends on their size and coating,³¹ investigations of other USPIO agents have demonstrated a higher uptake per gram of tissue in the spleen than in the liver.^{16,32–34} Within the liver, it has been shown that ferumoxytol is taken up primarily by the Kupffer cells (the resident macrophages of the liver), with sparse uptake by the endothelial cells of the liver sinusoids and no uptake by hepatocytes.¹⁴ The Kupffer

cells, however, comprise only about 2.1% of the liver parenchyma by volume³⁵ and play a lesser role in iron storage than do hepatocytes, which represent about 78% of the parenchymal volume.³⁵ Evidence from animal studies suggests that the Kupffer cells break down USPIO particles over a period of several days and export much of the iron in the form of ferritin and transferrin, which are then absorbed by hepatocytes.^{36,37} This process of iron transfer between the Kupffer cells and hepatocytes has also been observed after erythrophagocytosis.³⁸ On the basis of this evidence and our own results, we infer that ferumoxytol particles are phagocytosed and catabolized by macrophages both in the spleen and in the liver, but that much of the iron extracted from the particle core is transported to hepatocytes for long-term storage. This would explain the large R2 and R2* responses observed in the spleen and in the liver at 3 days and the greater recovery exhibited by the spleen than by the liver at 1 month.

It is of interest to consider whether our results are valid for other USPIO agents or whether they are unique to ferumoxytol. As described previously, the time taken for R2 and R2* recovery in the liver includes both the time taken for degradation of the particles and the time required for elimination of the iron released from the particle core. Although evidence suggests that the degradation rate of iron oxide particles is independent of particle size, it has been shown to depend strongly on coating³⁶; reported half-lives in rats range from 8 days for dextran-coated particles such as ferumoxides (Feridex/Endorem) and ferumoxtran-10 (Combidex/Sinerem) to 29 days for feruglose (NC100150/Clariscan), which has a coating of pegylated starch.³⁶ An MRI study in mice demonstrates that ferumoxytol closely resembles ferumoxides in this regard.¹⁴ However, these differences may be a minor factor in humans because our data suggest that the time taken for particle degradation in humans is short compared with the time required for subsequent elimination of the iron released from the particle core. Because the clearance rate for excess iron should depend only on the body's iron metabolism and not on properties of the original particles, it follows that our results for R2 and R2* recovery in the liver should be largely applicable to other iron oxide particles, provided the agents are administered at the same dose. Smaller doses of iron are expected to clear more quickly.¹⁵

Because USPIO particles are taken up primarily by macrophages, it is reasonable to suppose that the integrated 3-day response among all organs of the mononuclear phagocyte system should be proportional to the total dose administered. We observed statistically significant correlations between the net dose of ferumoxytol in units of milligrams of iron and the 3-day R2 and R2* responses integrated over the liver and the spleen. Although ferumoxytol is also known to be taken up by hematopoietic bone marrow,³⁹ we were not able to include the contribution of the bone marrow in our calculations because we did not survey the axial skeleton. The fact that we observed significant correlations without taking the bone marrow into account may suggest that the liver and the spleen take up most of the ferumoxytol particles or that the net uptake by the bone marrow was independently correlated with iron dose as calculated from body weight.

The main limitation of this study was the small number of participants. Further studies with larger cohorts and different iron doses would provide better characterization of iron clearance rates. Investigation of the physiological and genetic basis underlying the variation in iron elimination, however, is beyond the scope of this MRI approach.

In conclusion, we have shown that the rate of iron clearance after ferumoxytol administration in healthy adults varies greatly among individuals but that complete elimination of a dose of 5 mg Fe/kg may take more than 11 months. Much of the excess iron is stored in the liver, where it alters signal contrast on MR images, mimicking iron overload disorders and potentially complicating estimation of liver fat for several months after administration. This is an

important consideration in the use of ferumoxytol and other USPIO particles as contrast agents for diagnostic imaging.

REFERENCES

- Corot C, Robert P, Idee JM, et al. Recent advances in iron oxide nanocrystal technology for medical imaging. *Adv Drug Deliv Rev.* 2006;58:1471–1504.
- Islam T, Harisinghani MG. Overview of nanoparticle use in cancer imaging. *Cancer Biomark.* 2009;5:61–67.
- Wu L, Cao Y, Liao C, et al. Diagnostic performance of USPIO-enhanced MRI for lymph-node metastases in different body regions: a meta-analysis. *Eur J Radiol.* 2011;80:582–589.
- Harnan SE, Cooper KL, Meng Y, et al. Magnetic resonance for assessment of axillary lymph node status in early breast cancer: a systematic review and meta-analysis. *Eur J Surg Oncol.* 2011;37:928–936.
- Corot C, Petry KG, Trivedi R, et al. Macrophage imaging in central nervous system and in carotid atherosclerotic plaque using ultrasmall superparamagnetic iron oxide in magnetic resonance imaging. *Invest Radiol.* 2004;39:619–625.
- Tang TY, Muller KH, Graves MJ, et al. Iron oxide particles for atheroma imaging. *Arterioscler Thromb Vasc Biol.* 2009;29:1001–1008.
- Ho C, Hitchens TK. A non-invasive approach to detecting organ rejection by MRI: monitoring the accumulation of immune cells at the transplanted organ. *Curr Pharm Biotechnol.* 2004;5:551–566.
- Metz S, Beer AJ, Settles M, et al. Characterization of carotid artery plaques with USPIO-enhanced MRI: assessment of inflammation and vascularity as in vivo imaging biomarkers for plaque vulnerability. *Int J Cardiovasc Imaging.* 2011;27:901–912.
- Tang TY, Howarth SP, Miller SR, et al. The ATHEROMA (Atorvastatin Therapy: Effects on Reduction of Macrophage Activity) Study: evaluation using ultrasmall superparamagnetic iron oxide-enhanced magnetic resonance imaging in carotid disease. *J Am Coll Cardiol.* 2009;53:2039–2050.
- Hauger O, Grenier N, Deminere C, et al. USPIO-enhanced MR imaging of macrophage infiltration in native and transplanted kidneys: initial results in humans. *Eur Radiol.* 2007;17:2898–2907.
- Wu YL, Ye Q, Sato K, et al. Noninvasive evaluation of cardiac allograft rejection by cellular and functional cardiac magnetic resonance. *JACC Cardiovasc Imaging.* 2009;2:731–741.
- Ganz T, Nemeth E. Hepcidin and iron homeostasis. *Biochim Biophys Acta.* 2012;1823:1434–1443.
- Sebastiani G, Pantopoulos K. Disorders associated with systemic or local iron overload: from pathophysiology to clinical practice. *Metalomics.* 2011;3: 971–986;1823.
- Kalber TL, Smith CJ, Howe FA, et al. A longitudinal study of R2* and R2 magnetic resonance imaging relaxation rate measurements in murine liver after a single administration of 3 different iron oxide-based contrast agents. *Invest Radiol.* 2005;40:784–791.
- Briley-Saebo K, Hustvedt SO, Haldorsen A, et al. Long-term imaging effects in rat liver after a single injection of an iron oxide nanoparticle based MR contrast agent. *J Magn Reson Imaging.* 2004;20:622–631.
- Bourrinet P, Bengeli HH, Bonnemain B, et al. Preclinical safety and pharmacokinetic profile of ferumoxtran-10, an ultrasmall superparamagnetic iron oxide magnetic resonance contrast agent. *Invest Radiol.* 2006;41:313–324.
- Stabi KL, Bendz LM. Ferumoxytol use as an intravenous contrast agent for magnetic resonance angiography. *Ann Pharmacother.* 2011;45:1571–1575.
- Neuwelt EA, Hamilton BE, Varallyay CG, et al. Ultrasmall superparamagnetic iron oxides (USPIOs): a future alternative magnetic resonance (MR) contrast agent for patients at risk for nephrogenic systemic fibrosis (NSF)? *Kidney Int.* 2009;75:465–474.
- Wood JC. Impact of iron assessment by MRI. *Hematology Am Soc Hematol Educ Program.* 2011;2011:443–450.
- Tziomalos K, Perifanis V. Liver iron content determination by magnetic resonance imaging. *World J Gastroenterol.* 2010;16:1587–1597.
- Chandarana H, Lim RP, Jensen JH, et al. Hepatic iron deposition in patients with liver disease: preliminary experience with breath-hold multiecho T2*-weighted sequence. *AJR Am J Roentgenol.* 2009;193:1261–1267.
- Pai AB, Nielsen JC, Kausz A, et al. Plasma pharmacokinetics of two consecutive doses of ferumoxytol in healthy subjects. *Clin Pharmacol Ther.* 2010; 88:237–242.
- Bishara AJ, Hittner JB. Testing the significance of a correlation with nonnormal data: comparison of Pearson, Spearman, transformation, and resampling approaches. *Psychol Methods.* 2012;17:399–417.
- Gossuin Y, Gillis P, Muller RN, et al. Relaxation by clustered ferritin: a model for ferritin-induced relaxation in vivo. *NMR Biomed.* 2007;20:749–756.
- Gossuin Y, Gillis P, Hocq A, et al. Magnetic resonance relaxation properties of superparamagnetic particles. *Wiley Interdiscip Rev Nanomed Nanobiotechnol.* 2009;1:299–310.
- Wood JC, Enriquez C, Ghugre N, et al. MRI R2 and R2* mapping accurately estimates hepatic iron concentration in transfusion-dependent thalassemia and sickle cell disease patients. *Blood.* 2005;106:1460–1465.
- Ghugre NR, Wood JC. Relaxivity-iron calibration in hepatic iron overload: probing underlying biophysical mechanisms using a Monte Carlo model. *Magn Reson Med.* 2011;65:837–847.
- MacKenzie EL, Iwasaki K, Tsuji Y. Intracellular iron transport and storage: from molecular mechanisms to health implications. *Antioxid Redox Signal.* 2008;10:997–1030.
- Sirlin CB. Invited commentary. *Radiographics.* 2009;29:1277–1280.
- Hanna RF, Kased N, Kwan SW, et al. Double-contrast MRI for accurate staging of hepatocellular carcinoma in patients with cirrhosis. *AJR Am J Roentgenol.* 2008;190:47–57.
- Chouly C, Pouliquen D, Lucet I, et al. Development of superparamagnetic nanoparticles for MRI: effect of particle size, charge and surface nature on biodistribution. *J Microencapsul.* 1996;13:245–255.
- Weissleder R, Elizondo G, Wittenberg J, et al. Ultrasmall superparamagnetic iron oxide: characterization of a new class of contrast agents for MR imaging. *Radiology.* 1990;175:489–493.
- Bengele HH, Palmacci S, Rogers J, et al. Biodistribution of an ultrasmall superparamagnetic iron oxide colloid, BMS 180549, by different routes of administration. *Magn Reson Imaging.* 1994;12:433–442.
- Rety F, Clement O, Siauve N, et al. MR lymphography using iron oxide nanoparticles in rats: pharmacokinetics in the lymphatic system after intravenous injection. *J Magn Reson Imaging.* 2000;12:734–739.
- Blouin A, Bolender RP, Weibel ER. Distribution of organelles and membranes between hepatocytes and nonhepatocytes in the rat liver parenchyma: a stereological study. *J Cell Biol.* 1977;72:441–455.
- Briley-Saebo KC, Johansson LO, Hustvedt SO, et al. Clearance of iron oxide particles in rat liver: effect of hydrated particle size and coating material on liver metabolism. *Invest Radiol.* 2006;41:560–571.
- Briley-Saebo K, Björnerud A, Grant D, et al. Hepatic cellular distribution and degradation of iron oxide nanoparticles following single intravenous injection in rats: implications for magnetic resonance imaging. *Cell Tissue Res.* 2004; 316:315–323.
- Sibile JC, Kondo H, Aisen P. Interactions between isolated hepatocytes and Kupffer cells in iron metabolism: a possible role for ferritin as an iron carrier protein. *Hepatology.* 1988;8:296–301.
- Simon GH, Raatschen HJ, Wendland MF, et al. Ultrasmall superparamagnetic iron-oxide-enhanced MR imaging of normal bone marrow in rodents: original research original research. *Acad Radiol.* 2005;12:1190–1197.